Numerical precision and dissipation errors in rotating flows

P.G. Tucker

Department of Applied Physics, Electronic and Mechanical Engineering, University of Dundee, Dundee, UK

Received February 1996
Accepted June 1996

Nomenclature

a, b	= inner and outer radii
c_p	= specific heat
g	= acceleration due to earth's gravity
k	= thermal conductivity
$L = r - a$	= radial distance measured from a; or characteristic length
n	= normal to a surface; or coefficient
P	= static pressure
p	= reduced static pressure
q	= general variable
Δq	= change in general variable
r, θ, z	= radial, tangential and axial co-ordinates respectively
S	= source term
s	= width of fluid enclosure
T	= temperature
$T' = T/T_{max}$	= dimensionless temperature
t	= time
$t' = \Omega t$	= dimensionless time
Δt	= time step
$\Delta t' = \Omega \Delta t$	= dimensionless time step
$\boldsymbol{u}$	= velocity vector
u, v, w	= radial, tangential and axial velocity components, respectively
W	= bulk average axial velocity
α_0, α_1	= relaxation parameters
μ	= dynamic viscosity
ρ	= density
Ω	= angular velocity of enclosure
ω	= angular velocity of co-ordinate system
τ	= stream function
$\tau' = \tau\rho/\mu$	= dimensionless stream function
Γ	= diffusion coefficient

Subscripts

q	= pertaining to general variable
max	= maximum value
s	= pertaining to surface
i, o	= pertaining to inlet and outlet values respectively

Introduction

Prediction of three-dimensional, rotating flows is important for turbomachinery design, and the study of oceans and the earth's atmosphere (geophysical flows). Computational fluid dynamics (CFD) is emerging as a popular predictive technique, with many applications in these areas. Generally, when computing rotating flows, the co-ordinate system angular velocity ω is chosen so that $\Omega \geq \omega \geq 0$ (e.g. [1-3]), where Ω is a system boundary angular velocity. Here the effect of ω, on predictions, is illustrated with three, cylindrical polar co-ordinate (r, θ, z) examples. Two extremes in choices of ω are used: $\omega = 0$ and $\omega = \Omega$. Geophysical flows[4,5] and those found in certain cylindrical turbomachinery cavities[6,7] are complex, unsteady and non-axisymmetric ($\partial q/\partial\theta \neq 0$, where $q = \boldsymbol{u}, p, T, \rho$ and μ, and $\boldsymbol{u}$ is a velocity vector, p pressure, T temperature, ρ density and μ dynamic viscosity). Predicting these complex flows can be challenging to the numerical modeller. Attention must be paid to numerical precision and other discretization aspects.

The author would like to thank Drs Chris Long and Patrick Keogh for their helpful discussions on this work.

International Journal for Numerical Methods for Heat & Fluid Flow
Vol. 7 No. 7, 1997, pp. 647–658.

Numerical precision

For geophysical flows, the hydrostatic pressure, $\rho g z$ (where g is the acceleration due to gravity and z depth) can be large, relative to flow driving pressure differences. To see the detrimental effect of this hydrostatic pressure gradient, it is helpful to consider the linear inviscid momentum equations in a polar (r, θ) co-ordinate system. These are given below:

$$-2\omega v = \frac{1}{\rho}\frac{\partial p}{\partial r}, 2\omega u = \frac{1}{\rho r}\frac{\partial p}{\partial \theta}, \quad (1)$$

where p is some reduced pressure, discussed later, and u and v radial and tangential velocity components relative to a co-ordinate system rotating at ω. As can be seen from equation (1), prediction of r, θ plane velocity components depends on accurate modelling of pressure gradients. Consequently, a hydrostatically reduced pressure is used when predicting this type of flow[4,5]. Without this, axisymmetric solutions can result and so clearly, numerical precision is important. When solving for v, higher numerical precision is also gained if ω is chosen so that, on average, v is small. However, in turbomachinery, where rotating surfaces are often close to stationary surfaces[2] the choice of ω, to minimize v, is not always obvious.

Numerical dissipation

For relatively high Reynolds number flow solutions, a CFD practice is to raise viscosity levels artificially. This increases dissipation/diffusion, smoothing dependent variable variations. The increased dissipation is sometimes described as false[8] or numerical[9].

Numerous convective term discretizations have been developed to try to reduce numerical dissipation and maintain stability. A review of many of these, applied to turbulent flows, is given by Leschziner[10]. Studies on the performance of schemes of this type have been made by workers such as Huang *et al.*[11], Patel and Markatos[12], Vanka[13] and Smith and Hutton[14]. It is not clear from these investigations which method is best. This is especially the case since none of them were applied to rotating flows. Considering just the tangential flow components, the HYBRID and CONDIF schemes of Spalding[15] and Runchal[16], respectively introduce numerical dissipation when relative local cell Peclet ($Pe = \rho v L/\Gamma$, where Γ is a diffusion coefficient and L a control volume characteristic length) numbers become greater than 2. For $Pe \leq 2$ these schemes use non-dissipative central differencing. Setting ω to minimize the average value of v, and hence Pe produces less numerical dissipation and higher accuracy. As can be seen from this discussion, co-ordinate system angular velocity is related to numerical precision, dissipation and consequently solution accuracy.

Example details

To illustrate the effect of ω, unsteady, non-isothermal, three-dimensional flow examples relevant to turbine engines and the earth's atmosphere are chosen.

Example I is the flow in an idealized cavity, rotating at Ω, with an axial throughflow of air (see Figure 1). This geometry, shown in Figure 1a, is used by Iacovides and Chew[17] and Farthing *et al.*[7] to study fluid flow in modern gas turbine aero engine high pressure compressor spool cavities. The cavity consists of two pierced discs of outer radius *b* and inner radius *a*, connected by a cylindrical shroud of width *s*. Experiments by Farthing *et al.* show the flow, for this configuration (see Figure 1b), can consist of a radial fluid arm, emanating from the axial throughflow air, flanked by a cyclone and anticyclone. A separation zone, where no axial throughflow entered, was also observed.

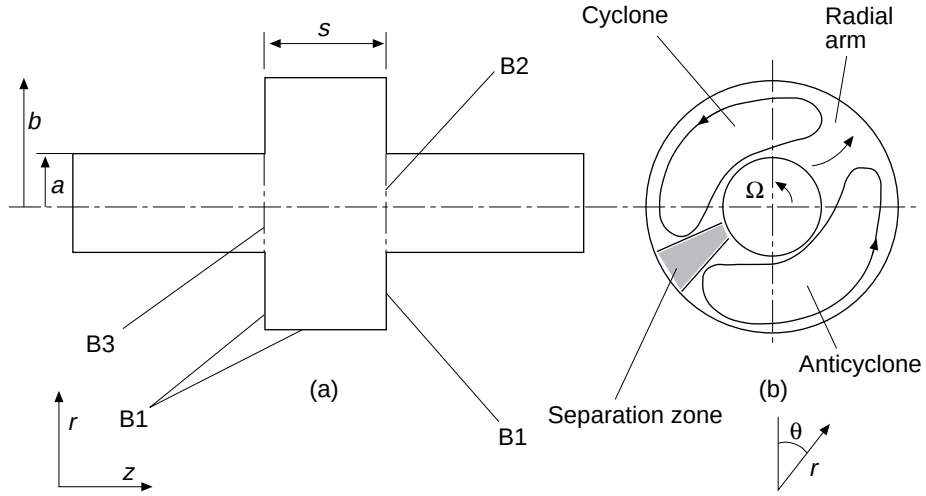

Figure 1. Rotating cavity with an axial throughflow: (a) geometry and boundary conditions ($r-z$ plane); (b) flow structure ($r-\theta$ plane)

Example II is the flow in an annulus, of length *s*, with an outer radius of *b* and inner *a*, shown in Figure 2. The earth's acceleration due to gravity *g*, acts parallel to the axis of rotation. There is a temperature difference between the inner and outer cylinders. This simple configuration for studying atmospheric flows was proposed by Thomson in 1892 and is still used (see [4,18]). A typical annulus flow structure, consisting of a jet flanked by cyclones and anticyclones, is shown in Figure 2b.

Example III is the heat transport in a hydrodynamic journal bearing with an orbiting shaft of radius *a*, shown in Figure 3. The orbit is circular, having an angular velocity Ω equal to that of the shaft. The bearing has an outer radius *b* and width *s*. Importantly, the orbit results in the same point on the shaft being closest to the bearing and hence receiving most heating. As observed by de Jongh and Morton[19], and analytically demonstrated Keogh and Morton[20], this can cause a significant diametrical shaft temperature gradient, thermal bending and eventual gas turbine engine failure.

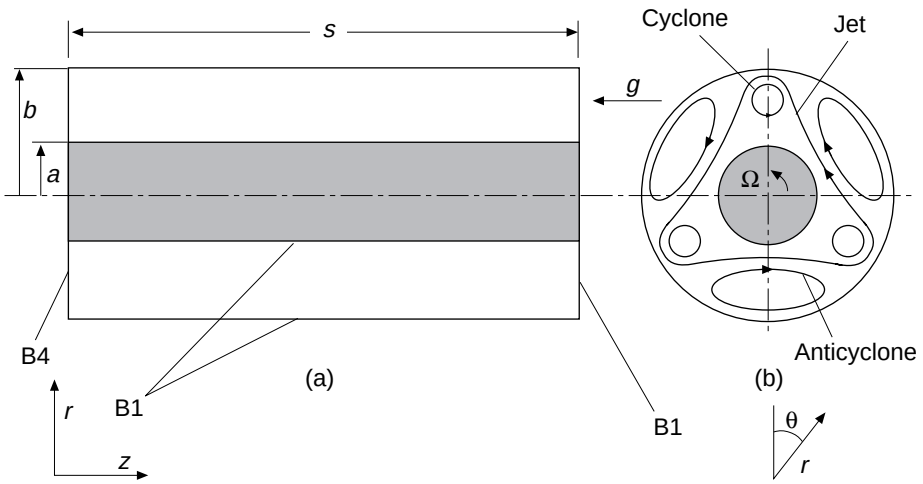

Figure 2.
Rotating annulus: (a) geometry and boundary conditions ($r - z$ plane); (b) flow structure ($r - \theta$ plane)

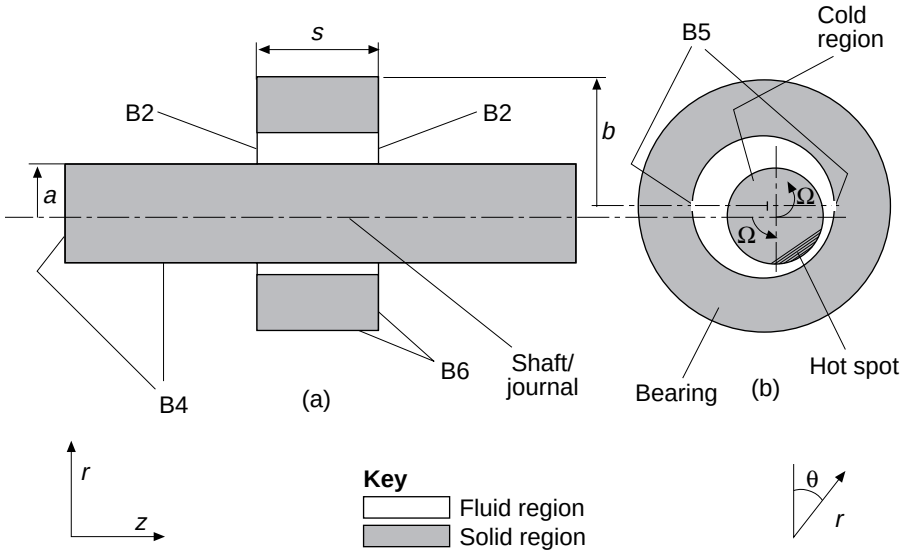

Figure 3.
Hydrodynamic journal bearing with an orbiting shaft: (a) geometry and boundary conditions ($r - z$ plane); (b) geometry, boundary conditions, and hot and cold regions ($r - \theta$ plane)

Numerical method

Governing equations

The momentum and energy equations can be written in the common general form:

$$\frac{\partial}{\partial t}(\rho q) + \nabla.(\rho \mathbf{u} q) = \nabla.(\Gamma_q \nabla q) + S_q \tag{2}$$

where q is either a velocity component or temperature, S_q a source term containing products and gradients of variables, Γ_q a diffusion coefficient, t time and $\boldsymbol{u}$ a velocity vector. The exact form of the operators and source terms used

in equation (2) are given by Tucker and Keogh[21]. The continuity equation can be written as:

$$\frac{\partial \rho}{\partial t} + \nabla .(\rho \mathbf{u}) = 0 \tag{3}$$

In Example III, the fluid (oil) cannot withstand negative pressure and cavitates, producing an oil and gas mixture. Where cavitation occurs ($p < 0$ N/m^2, gauge), harmonic means of ρ and Γ_q, based on the radially averaged fractions of oil and gas are taken. The fraction of oil $q(\theta, z, t)$ in the cavitated region is calculated, from conservation of mass considerations, using

$$\frac{\partial}{\partial t}\left(Lq\right) + \nabla .(\int_a^{a+L} \mathbf{u} dr q) = 0 \tag{4}$$

where $L(\theta, t)$ is the radial distance between the bearing inner surface and shaft. Full details of this cavitation model are given by Tucker and Keogh[21].

Solution of governing equations

The solution of equations (2)-(4) is based on the staggered grid technique described by Patankar[8]. A reduced pressure field

$$p = P - n\rho g z - \frac{1}{2} \rho \Omega^2 r^2 \tag{5}$$

is solved for with the SIMPLEC algorithm of Van Doormaal and Raithby[22], where $n = 1$ for Example II and $n = 0$ for all others. The HYBRID, CONDIF and central difference schemes, discussed in the introduction, are used as convective term treatments. For Examples I and III, an implicit time scheme is used, but for Example II a second order trapezoidal time integration, described by Tucker and Long[5], is used.

Coupling between tangential and radial momentum equations is improved by adding the following term to S_u in the discretized form of equation (2)

$$-\alpha_0 \rho | v + \alpha_1 \Omega r | \frac{\Delta u}{r}, \tag{6}$$

where Δu is the difference in u between successive iterations, and α_0 and α_1 relaxation parameters. When $\alpha_1 = 1$ the term is identical to that proposed by Gosman *et al.*[23]. This coupling technique is preferred to the source term decomposition proposed by Jang and Acharya[24], which produced cpu time increases relative to solutions without any source term modification. Discretized equations are solved using a TDMA solver. In Example I, convergence is accelerated using a non-linear multigrid algorithm described by Tucker[25].

Convergence is assessed using *rms* changes, where

$$rms_q = \sqrt{\frac{\Sigma(\Delta q)^2}{\Sigma q^2}} \tag{7}$$

and Δq is the difference in q between successive iterations. In Examples I and II, each time step is taken as converged when the *rms* change, for all variables, is less than 2.5×10^{-5}. For the multiphase flow, Example III, a value of 1×10^{-4} is used.

The programme described has been validated for a wide range of complex, three dimensional, time dependent, non-isothermal, multiphase, moving boundary and conjugate, rotating flow cases. Much of this work is described in detail by Tucker[25], Tucker and Keogh[21,26] and Long and Tucker[27]. In most instances pleasing agreement is found with validation data.

Boundary conditions

Boundary conditions, identified in Figures 1-3, are summarized in Table I. The subscripts i, o and s are used to indicate inlet, outlet and surface, boundary conditions; and n is used to define a surface normal. For Example I, T_i = 293 K, $p_o = 1.03 \times 10^5$; and for $r \geq b$, T_s = 293 K, and $a < r < b$, T_s = 382-89 r/b. In Example II, at $r = a$, T_s = 295 K and when $r = b$, T_s = 299 K. For Example III, $p_i \approx 1.35 \times 10^5$ N/m^2, T_i = 50°C and T_s, in boundary condition B6, is a solution variable.

	Boundary condition
B1	$u = w = 0, v = \Omega r, T = T_s$
B2	$\frac{\partial u}{\partial n} = \frac{\partial v}{\partial n} = \frac{\partial w}{\partial n} = \frac{\partial T}{\partial n} = 0, p = p_o$
B3	$u = 0, v = \Omega r, w = W, T = T_i$
B4	$u = w = 0, v = \Omega r, \frac{\partial T}{\partial n} = 0$
B5	$v = w = 0, u$ – *set so mass concerved* $p = p_i, T = T_i$
B6	$\frac{\partial T}{\partial n} = (308 - T_s)$

Table I.
Numerical boundary conditions

Numerical parameter settings

The number of grid nodes in the fluid region, relaxation factors, dimensionless time steps $\Delta t' = \Omega \Delta t$ and approximate computing times, for each time step, are summarized in Table II. The computing times are for a SPARC Center 2000 with four 40 MHz processors, and the required storage is between 10 and 20Mb.

For Example III, the number of grid nodes in the solid bearing are the same as for the fluid region (see Table II). For the shaft a $29 \times 9 \times 40$ (z, r, θ) grid is

used. Grids are refined at boundaries using geometric expansions. For the fluid, established correlations are used to ensure two to three grid nodes are committed to boundary layers. Time steps are made sufficiently small to avoid the need for under relaxation. Predictions by Long and Tucker[27], Tucker and Long[5] and Tucker and Keogh[21,26], show the parameters in Table II, give (for the illustrative purposes of this paper) more than acceptable grid and time step independence of solutions.

Example	Axial nodes	Radial nodes	Tangential nodes	α_0	α_1	$\Delta t'$	Computer time(s)
I	17	21	40	2	2	0.85	300
II	28	22	60	0	0	0.1	250
III	9	5	40	10	1	0.015	100

Table II. Numerical parameter details

Physical dimensions

The characteristic dimensions a, b and s, and rotating surface angular velocities are summarized in Table III.

Example	a (m)	b (m)	s (m)	Ω (rad/s)
I	0.0108	0.108	0.0288	17.0168
II	0.025	0.08	0.14	1
III	0.05	0.1	0.055	367

Table III. Characteristic dimensions and angular velocities

In Example III, the shaft length is 0.45m, the orbit diameter 0.0357mm and the orbit centre 0.0398mm from the bearing centre, giving $L(\theta, t)_{\max} \approx 0.031$mm. Also, the diametrically opposite fluid inlets have an angular extent of 9° and an axial length of 0.0275m. For Examples I to III the working fluids are air, a water/glycerol mixture and oil respectively. Properties are given in the Appendix.

Form of results presentation

All contour plots are presented in the midaxial $r - \theta$ plane. For Examples I and II contours are of a dimensionless stream function

$$\tau' = \frac{\tau\rho}{\mu}. \tag{8}$$

Velocity components are related to τ' by the following relationships

$$v = -\frac{\partial}{\partial r}\left(\frac{\tau'\mu}{\rho}\right), u = \frac{1}{r}\frac{\partial}{\partial\theta}\left(\frac{\tau'\mu}{\rho}\right). \tag{9}$$

Despite the flow being three dimensional, this two dimensional stream function definition is revealing and illustrates the point to be made here. For Example III, contours of the dimensionless temperature

$$T' = \frac{T}{T_{max}} \tag{10}$$

are used, where T_{max} is a maximum temperature.

Discussion of results

For Examples I, II and III the Peclet numbers associated with the tangential co-ordinate direction/energy equation, in a stationary co-ordinate system ($\omega = 0$), are on average approximately (assuming solid body rotation, which is true to within 2 per cent) 300, 1,500, and 3,000 respectively. For $\omega = 0$, to eliminate numerical dissipation (making $Pe < 2$) from HYBRID and CONDIF solutions, would require 6,000, 30,000 and 60,000 tangential grid nodes, for Examples I, II and III respectively. As can be seen, all HYBRID and CONDIF solutions presented here with $\omega = 0$ will have numerical dissipation.

For Example I, the variation of τ', at $t' \approx 350$, using the HYBRID scheme, is shown in Figure 4. Figures 4a and b show the predicted flow for $\omega = \Omega$ (a rotating co-ordinate system) and $\omega = 0$ respectively. In Figure 4a, cyclone/anticyclone regions, a radial arm and evidence of the separation zone identified by Farthing *et al.* (cf. Figure 1b) can be seen. For $\omega = 0$ (Figure 4b) the solution is axisymmetric ($\partial q/\partial\theta = 0$). This axisymmetric solution still results when the CONDIF and central difference schemes are used. Since the central difference scheme is not numerically dissipative and CONDIF not highly dissipative, numerical precision, rather than dissipation, is causing the erroneous axisymmetric prediction.

Figure 5 illustrates the variation of τ', for Example II, at $t' \approx 1{,}000$ using the HYBRID scheme. Figures 5a and 5b show the predicted flow for $\omega = \Omega$ and $\omega =$

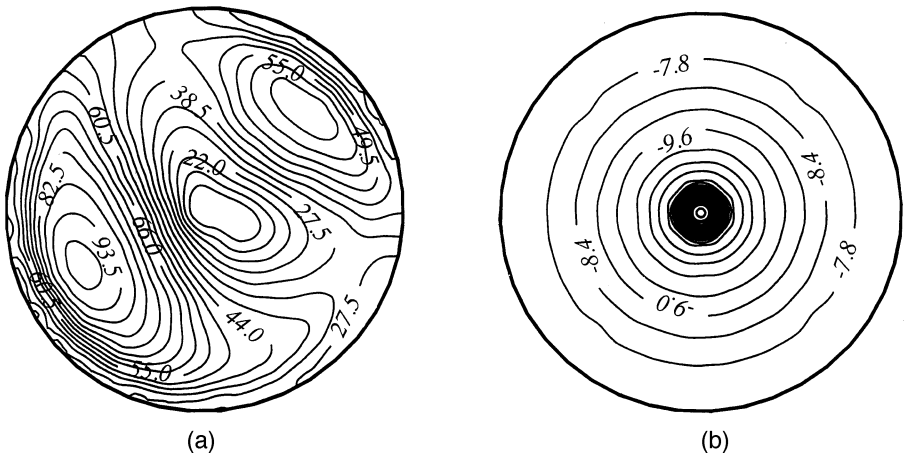

Figure 4.
Variation of τ', for Example I, at $t' \approx 350$, using HYBRID scheme: (a) $\omega = \Omega$ and (b) $\omega = 0$

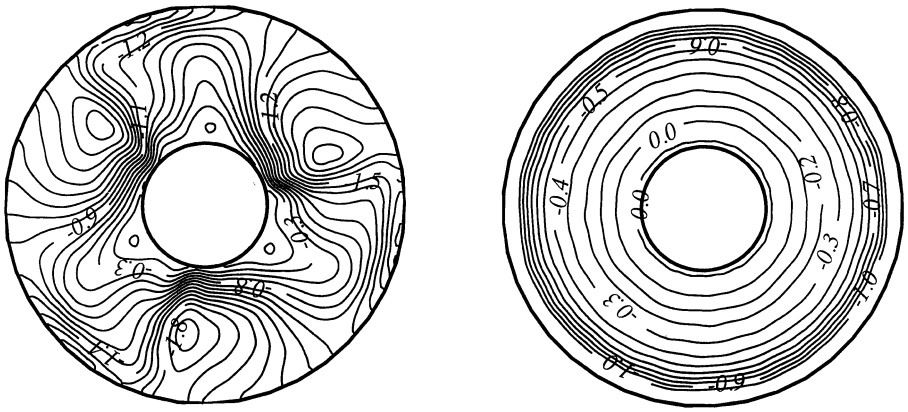

Figure 5. Variation of τ', for Example II, at $t' \approx 1{,}000$, using HYBRID scheme: (a) $\omega = \Omega$ and (b) $\omega = 0$

0, respectively. The flow shown in Figure 5a has the characteristics observed in Hignett *et al.*'s experiments (cf. Figure 2b) for the same condition. There are three cyclone/anticyclone pairs between which a fast moving jet passes. Comparisons (see [5]) with velocity measurements of Hignett *et al.* show pleasing agreement. The hydrostatic pressure distribution ($\rho\, g\, z$) is large relative to flow driving pressure differences. Owing to the limited computer precision, the reduced pressure defined by equation (5), must be solved for, otherwise $\partial q/\partial\theta = 0$. The prediction must also be made with $\omega = \Omega$; since if $\omega = 0$ errors result (see Figure 5b). For $\omega = 0$, the central difference scheme, although producing a significant accuracy loss with some pointwise oscillations, gives a solution having the features observed by Hignett *et al.* This suggests the major error in Figure 5b when $\omega = 0$ is due to numerical dissipation and not precision.

Figure 6 shows the variation of T' for Example III (hydrodynamic journal bearing) involving the HYBRID scheme. Figure 6a, with $\omega = \Omega$, clearly shows

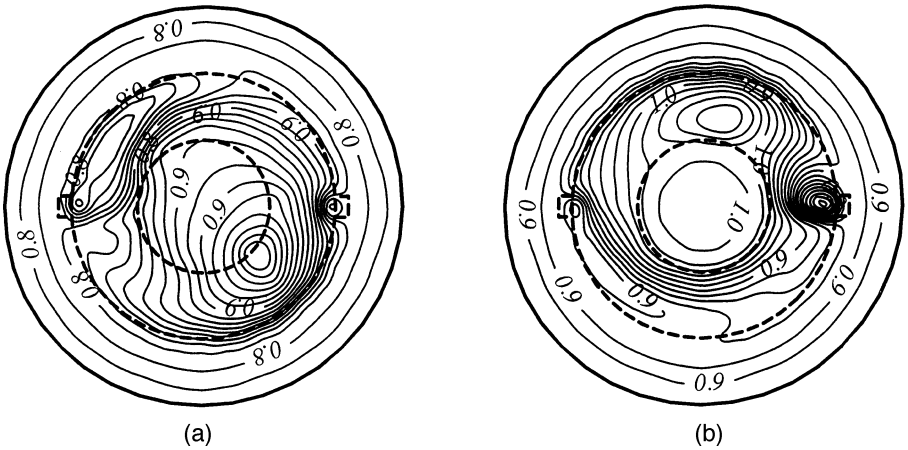

Figure 6. Variation of T', for Example III, involving HYBRID scheme: (a) $\omega = \Omega$ and (b) $\omega = 0$

that in the shaft $\partial q/\partial\theta > 0$, which is consistent with the observations of de Jongh and Morton[19] and Keogh and Morton[20]. However, as shown in Figure 6b, when $\omega = 0$, $\partial T/\partial\theta = 0$. With $\omega = 0$, Pe is too high to gain converged central difference solutions. However, numerical experiments, reducing the tangential grid spacing $\Delta\theta$, and hence numerical dissipation, gave $\partial T/\partial\theta > 0$ suggesting that, again, for $\omega = 0$ and high Peclet numbers, numerical dissipation is the most significant cause of error. This is to be expected, since the shaft temperature field is governed essentially by a conduction of heat equation ($\Omega\partial T/\partial\theta = \Gamma_T\nabla^2 T$); the solution of which is unlikely to be greatly influenced by numerical precision.

As can be seen, for design engineering, careful consideration should be given to the value of ω. For the examples presented, where all surfaces have the same angular velocity, $\omega = \Omega$ gave the greatest accuracy, relative to $\omega = 0$. For other configurations, the choice of ω is not clear. In certain aero engine cavities with stationary and rotating discs $\partial q/\partial\theta > 0$ (see [6]). For these cavities, the choice of ω, to minimize v (increasing numerical precision) and Pe (reducing numerical dissipation), is not obvious. Perhaps the average angular velocity of the two discs ($\omega = \Omega/2$) would give acceptable accuracy. For hydrodynamic journal bearings, similar to Example III, Tucker and Keogh[21] solve the stationary bearing/fluid and rotating shaft regions with $\omega = 0$ and $\omega = \Omega$ respectively. Using this sliding grid strategy, numerical precision is kept to a maximum, with Peclet numbers and hence dissipation to a minimum. The technique has the complexity of matching two different co-ordinate systems but offers potential.

Conclusions

The influence of numerical precision and dissipation has been illustrated using three, non-isothermal, unsteady, three-dimensional cylindrical rotating flow examples. Example I was the flow in a rotating cavity with an axial throughflow of air. The flow for this configuration is representative of that found in the high pressure compressor spool of a modern gas turbine aero engine. Example II was the flow in an annulus, where the earth's acceleration due to gravity acts parallel to the rotational axis. This configuration is used for the study of atmospheric flow mechanisms. Example III was the heat transport in a hydrodynamic journal bearing with an orbiting shaft.

For Example II, it was noted that relatively high hydrostatic pressures could reduce numerical precision causing incorrect axisymmetric predictions. For all examples it was noted that numerical precision increases and dissipation decreases when the co-ordinate system angular velocity ω is chosen to minimize relative tangential velocity.

Governing equations were solved using a staggered grid technique, utilizing the SIMPLEC pressure correction algorithm along with HYBRID, CONDIF and central difference convective term treatments. For Examples I and III an implicit time scheme was used, but for Example II a second order trapezoidal scheme was implemented. In Example III the fluid cavitated. Where cavitation occurred harmonic means of fluid and gas properties were used. Results were presented

in the form of contour plots in mid-axial $r - \theta$, planes for $\omega = 0$ (a stationary co-ordinate system) and $\omega = \Omega$ (a co-ordinate system rotating at the enclosure angular velocity Ω). The Peclet numbers associated with the tangential co-ordinate direction increased from Examples I to III.

When $\omega = \Omega$, all predictions agreed with experimental observations. However, for Example I, with, on average, the lowest tangential Peclet numbers, when $\omega = 0$, poor numerical precision caused an erroneous axisymmetric prediction. For Example II, where Peclet numbers are approximately a factor of five higher, when $\omega = 0$, HYBRID scheme numerical dissipation resulted in an erroneous axisymmetric prediction. Similarly, for Example III, with the highest Peclet numbers, $\omega = 0$ again gave an erroneous axisymmetric solution, which computations suggest is due to numerical dissipation.

As can be seen, careful consideration should be given to the choice of ω. Clearly, for the examples presented, $\omega = \Omega$ is best; but for other rotating systems the choice is not clear and further research is required.

References

1. Chew, J.W., "Computation of convective laminar flow in rotating cavities", *J. Fluid Mech.*, Vol. 153, 1985, p. 339.
2. Vaughan, C.M. and Turner, A.B., "Numerical predictions of axisymmetric flow in a rotor-stator system with external main stream flow", *Proc. 5th Int. Conf. Num. Meth. Lam. and Turb. Flow*, Pineridge Press, Montreal, 1987, p. 1640.
3. Tucker, P.G. and Long, C.A., "CFD prediction of vortex breakdown in a rotating cavity with an axial throughflow of air", *Int. Communications in Heat and Mass Transfer*, Vol. 22, No 5, 1995, p. 639.
4. Hignett, P., White, A.A., Carter, R.D., Jackson, W.D.N. and Small, R.M., "A comparison of laboratory measurements and numerical simulations of baroclinic wave flow in a rotating cylindrical annulus", *Quart. J. R. Met. Soc.*, Vol. 111, 1985, p. 131.
5. Tucker, P.G. and Long, C.A., "Second order finite volume jet stream computations", Accepted for publication in the *Int. J. of Num. Meths for Heat and Fluid Flow*, 1995.
6. Nordquist, J., Abrahamson, S., Wechkin, J. and Eaton, J., "1990 visualization studies in rotating disk cavity flows", *ASME J. of Turbomachinery*, Vol. 112, 1990, p. 308.
7. Farthing, P.R., Long, C.A., Owen, J.M. and Pincombe, J.R., "Rotating cavity with an axial throughflow of cooling air: flow structure", *ASME J. Turbomachinery*, Vol. 114, 1992, p. 237.
8. Patankar, S.V., *Numerical Heat Transfer and Fluid Flow*, Hemisphere, New York, NY, 1980.
9. Anderson, J.D., *Computational Fluid Dynamics: The Basics with Applications*, McGraw-Hill, New York, NY, 1995.
10. Leschziner, M.A., "Modelling turbulent recirculating flows by finite-volume methods – current status and future directions", *Int J. Heat and Fluid Flow*, Vol. 10, 1989, p. 186.
11. Huang, P.G., Launder, B.E. and Leschziner, M.A., "Discretization of nonlinear convection processes: a broad-range comparison of four schemes", *Computer Methods in Applied Mechanics and Engineering*, Vol. 48, 1985, p. 1.
12. Patel, M.K and Markatos, N.C., "An evaluation of eight discretization schemes for two-dimensional convection-diffusion equations", *Int J. for Num. Meths. in Fluids*, Vol. 6, 1986, p. 129.
13. Vanka, S.P., "Second-order upwind differencing in recirculating flow", *AIAA J.*, Vol. 25, 1987, p. 1435.

14. Smith, R.M. and Hutton, A.G., "The numerical treatment of advection: a performance comparison of current methods", *Num. Heat Transfer*, Vol. 5, 1982, p. 439.
15. Spalding, D.B., "A novel finite difference formulation for differential expressions involving both first and second derivatives", *Int. J. for Num. Meths. Engng.*, Vol. 4, 1972, p. 551.
16. Runchal, A.K., "CONDIF: a modified central-difference scheme for convective flows", *Int. J. for Num. Meths. Engng.*, Vol. 24, 1987, p. 1593.
17. Iacovides, H. and Chew, J.W., "The computation of convective heat transfer in rotating cavities", *Int. J. of Heat and Fluid Flow*, Vol. 14 No. 2, 1993, p. 146.
18. Nezlin, M. V. and Sutyrin, G.G., "Problems of simulation of large long-lived vortices in the atmospheres of the giant planets (Jupiter, Saturn, Neptune)", *Surv. in Geophys.*, Vol. 15, 1994, p. 63.
19. de Jongh, F.M. and Morton, PG., "The synchronous instability of a compressor rotor due to bearing journal differential heating", *ASME Int. Gas Turbine and Aeroengine Cong. and Exp.*, The Hague, 13-16 June 1994.
20. Keogh, P.S. and Morton, P.G., "Journal bearing differential heating evaluation with influence on rotor dynamic behaviour", *Proc. R. Soc. Lond. A*, Vol. 441, 1993, p. 527.
21. Tucker, P.G. and Keogh, P.S., "On the dynamic thermal state in a hydrodynamic bearing with a whirling journal using CFD techniques", Accepted for publication in the *ASME J. of Tribology*, 1995.
22. Van Doormaal, J.P. and Raithby, G.D., "Enhancement of the SIMPLE method for predicting incompressible fluid flows", *Num. Heat Transfer*, Vol. 7, 1984, p. 147.
23. Gosman, A.D., Koosinlin, M.L., Lockwood, F.C. and Spalding, D.B., "Transfer of heat in rotating systems", *ASME Paper 76-GT-25*, 1976.
24. Jang, D.S. and Acharya, S., "Source term decomposition to improve convergence of swirling flow calculations", *AIAA J.*, Vol. 26 No. 3, 1988, p. 372.
25. Tucker, P.G., "Numerical and experimental investigation of flow structure and heat transfer in a rotating cavity with an axial throughflow of cooling air", DPhil thesis, School of Engineering, University of Sussex, 1993.
26. Tucker, P.G. and Keogh, P.S., "A generalised CFD approach for journal bearing performance prediction", *Proc. Instn Mech. Engrs, Part J: Journal of Engineering Tribology*, Vol. 209, 1995, p. 99.
27. Long, C.A. and Tucker, P.G., "Numerical computation of laminar flow in a heated rotating cavity with an axial throughflow of air", *Int. J. of Num. Meths for Heat and Fluid Flow*, Vol. 4 No. 4, 1994, p. 347.

Appendix

Fluid and solid properties, for Examples I-III, are summarized in Table AI. For Example III, the thermal conductivity, density and specific heat of the solid shaft and bearing are 50 W/mK, 7,850 kg/m^3 and 460 J/kg K respectively.

Example	ρ (kg/m^3)	μ (kg/ms)	k/c_p (kg/ms)
I	$\frac{p}{287 \times T}$	0.1817×10^{-4}	2.6×10^{-5}
II	$1043[1 - 3.07 \times 10^{-4}(T - 295)$ $- 7.83 \times 10^{-6}(T - 295)^2]$	$0.0017[1 - 2.8 \times 10^{-2}(T - 295)$ $- 6.7 \times 10^{-4}(T - 295)^2]$	1.34×10^{-4} $(1 + 2.33 \times 10^{-3}(T - 295))$
III	850	850×10^{-6} $\exp(2.61 \times 10^{8} T^{-3.12} - 0.8)$	7.5×10^{-5}

Table AI.
Fluid properties